Dynamics of molecular and polymeric interfaces probed with atomic beam scattering and scanning probe imaging

Ryan D. Brown, Qianqian Tong, James S. Becker, Miriam A. Freedman, Nataliya A. Yufa and S. J. Sibener*

Received 8th February 2012, Accepted 20th February 2012
DOI: 10.1039/c2fd20016c

The scattering of atomic and molecular beams from well-characterized surfaces is a useful method for studying the dynamics of gas-surface interactions, providing precise information on the energy and momentum exchange which occur in such encounters. We apply this technique to new systems including disordered films of macromolecules, complex interfaces of macromolecular systems, and hybrid organic-semiconductor interfaces. Time-lapse atomic force microscopy studies of diblock copolymer structural evolution and fluctuations complement the scattering data to give a more complete understanding of dynamical processes in these complex disordered films. Our new scattering findings quantitatively characterize changes in interfacial dynamics including confinement in thin films of poly(methyl methacrylate) and changes in the physical properties of poly(ethylene terephthalate) films as they transform from the glassy to their semicrystalline phase. Further measurements on a hybrid organic-semiconductor interface, methyl-terminated silicon (111), reveal that the surface thermal motion and gas-surface energy accommodation are dominated by local molecular vibrations while the interfacial lattice dynamics remain accessible through helium scattering. High temperature atomic force microscopy allows direct, real-time visualization of structural reorganization and defect migration in poly(styrene)-*block*-poly(methyl methacrylate) films, revealing details of film reorganization and thermal annealing. Moreover, we employed lithographically created channels to guide the alignment of polymer microdomains. This, in turn, allows direct observation of the mechanisms for diffusion and annihilation of dislocation and disclination defects. In summary, this paper elaborates on the power of combining atom scattering and scanning probe microscopy to interrogate the vibrational dynamics, energy accommodation, energy flow, and structural reorganization in complex interfaces.

1. Introduction

Since the discovery of atom diffraction from alkali halide interfaces,[1] atom scattering techniques have been extended from a method of observing structure and lattice dynamics of clean ordered interfaces[2,3] to increasingly complex systems. The successful application of helium atom scattering toward the investigation of defects,[4] adsorbate decoration,[5,6] and thin film interfaces[7,8] has directed the evolution of this method as a tool for characterizing the dynamic and structural properties of increasingly complex interfaces. Herein we present the extension of atomic

The James Franck Institute and Department of Chemistry, The University of Chicago, 929 E. 57th Street, Chicago, Illinois 60637, USA. E-mail: s-sibener@uchicago.edu

scattering studies to include disordered organic films of macromolecules as well as complex ordered organic films. Our application of atom scattering to glassy and crystalline polymeric films as well as organically terminated semiconductor interfaces allows us to access interfacial vibrational dynamics and energy accommodation characteristics. Scanning probe microscopy techniques, specifically high temperature time-lapse atomic force microscopy, supplement the insight gained from atom scattering through real space visualization of the structural evolution and fluctuations in these disordered and structurally complex interfaces. The characterization of vibrational dynamics through atomic scattering combined with the real space visualization of complex polymer film evolution from atomic force microscopy gives us new insight into the vibrational dynamics and structural reorganization of disordered films on the atomic, nanoscopic, and microscopic length scales.

Neutral helium atom scattering (HAS) is a non-destructive and uniquely surface sensitive probe of surface structure and vibrations. Diffractive HAS arises due to the helium atom's de Broglie wavelength being on the order of an angstrom, which also imparts sensitivity to atomic scale fluctuations and vibrations. Helium's relatively light mass allows for the observation of small energy and momentum exchanges from collisions with a surface, and thus the low energy vibrations are accessible through time-of-flight scattering methods. Atomic scattering can be useful in characterizing interfacial vibrations through measuring the surface temperature dependence of the elastically scattered helium atoms as well as the single and multiple phonon energy exchanges between the helium atom and surface. Atomic force microscopy (AFM), specifically in an AC or tapping imaging configuration, is also a relatively non-perturbative scanning probe technique capable of visualizing real space events on the nanometer and micrometer length scales.

We begin this paper by demonstrating HAS's ability to detect subtle changes in vibrational dynamics of polymeric thin films through Debye–Waller attenuation measurements.[9] We find that the amplitudes of the surface mean-square displacements (MSD) normal to the surface plane are depressed for a 10 nm thick poly(methyl methacrylate), or PMMA, film relative to that of a thicker 50 nm film, and that this is corroborated by a suppression of annihilation events in the multiphonon lineshape. The sensitivity of the inelastic lineshape is investigated for chemical composition and molecular weight in other glassy polymers. Building upon these successes, we show that HAS is capable of examining the surface vibrational properties of poly(ethylene terephthalate) (PET) through temperature and angle sensitive Debye–Waller attenuation measurements, and that this method is capable of observing changes in surface dynamics arising due to a transition from a homogenous amorphous phase to a heterogeneous semi-crystalline phase. We observe a 15% enhancement in the amplitude of perpendicularly polarized MSDs for the semi-crystalline polymer, or a softening of these vibrational modes, yet a 25% suppression of the MSD amplitude in the surface plane. We can attribute these seemingly conflicting trends as features arising from different domains of this complex disordered surface.

We then move on to apply these Debye–Waller attenuation measurements to a methyl-terminated silicon interface in order to characterize the vibrational dynamics, energy accommodation, and gas-surface interaction potential. The CH_3–Si(111) interface exhibits thermal motion similar to a rigid semiconductor in the z direction, but in the surface plane its magnitude is closer to that of an alkanethiol SAM. We are able to use the angular dependence of the Debye–Waller factor to determine the helium-surface well depth and the surface Debye temperature. Further, we demonstrate the observation of single elastic vibrational modes of the underlying silicon lattice through single-phonon inelastic collision events for this complex surface. These measurements are capable of interrogating the dispersion relation of the underlying Si(111) lattice Rayleigh wave despite the presence of the covalently bound methyl overlayer.

Finally, we use time-lapse AFM to directly observe local structural fluctuations and reorganization in a complex diblock copolymer film. We present the observation of domain break up and reorganization and discuss how *in situ* imaging of this process lends insight into the mechanism of polymer diffusion in a poly(styrene)-*block*-poly(methyl methacrylate), PS-*b*-PMMA, film. Nanoconfinement of the diblock copolymer in channels causes alignment of the polymer domains in this film and allows direct observation of isolated defect interactions. These observations give insight into the mechanisms guiding defect migration and annealing for both dislocations and disclinations in these complex polymer films.

2. Experimental

Helium atom scattering experiments were performed using a high-energy and high-momentum resolution scattering apparatus which is described in detail elsewhere.[10] The apparatus can briefly be described as follows: A supersonic expansion of helium through a nozzle cooled by a closed cycle helium refrigerator giving a nearly monoenergetic beam of helium atoms with typical velocity distributions ($\Delta v/v$) of less than one percent. Time resolution is achieved by modulating the beam with a mechanical chopper. The beam was collimated to a 0.22° angular width and 4 mm spot size on a target mounted to a six-axis manipulator in the UHV scattering chamber, with a chopper-to-target distance of 0.5 m. The sample temperature is regulated by using a button heater to heat against cooling provided by a closed cycle helium refrigerator. The reflected atoms enter a differentially pumped rotatable detector with a target-to-ionizer flight path of 1 m for the PMMA, PS, and PB experiments and 0.5 m for the PET and methyl-terminated silicon experiments. The atoms are detected by ionization followed by mass selection.

The PMMA films were prepared by spin casting a solution of the polymer on Si(100) substrates with their native oxide. These films were annealed under argon to ensure uniformity, and film thickness was verified using ellipsometry. The PET films were prepared using a spin casting technique in which a PET solution was applied to a clean Au/Mica substrate, producing films of 80 nm depth. The film quality was verified with optical microscopy, and the film thickness was confirmed with ellipsometry and AFM. Upon completion of the scattering studies from the amorphous film, the sample was crystallized by annealing at 440 K for 30 min, which yielded films with a crystalline fraction of approximately 55% as confirmed by infrared reflection-absorption spectroscopy (IRRAS) measurements in a separate UHV chamber.[11]

The methylated silicon samples were prepared by the Lewis group at Caltech using their previously published method.[12] The functionalized wafers were transported from Pasadena to Chicago in sealed containers under inert atmosphere and loaded into the helium atom scattering apparatus. Angular scans were performed using a square wave chopping pattern with a 50% duty cycle and the rotatable detector arm (overall instrumental resolution 0.5°) was swept through the scan range under computer control. Energy-resolved time-of-flight measurements were performed using a single slit chopping pattern with a 1% duty cycle. The Debye–Waller attenuation experiments used a 46 meV beam and sample temperatures between 200 K and 500 K in 50 K steps, and the phonon spectroscopy experiments utilized beam energies of 43 to 65 meV and surface temperatures of 140 to 200 K. The Lewis group also prepared a set of deuterated methyl samples, CD_3–Si(111), so that the vibrational characteristics of this surface could be examined as well.

The atomic force microscopy experiments were performed using an Asylum MFP-3D atomic force microscopy with commercial silicon cantilevers and a polymer heater mount. We employed Olympus ACT160TS silicon cantilevers ($k \sim 42$ N m^{-1}) for imaging domain reorganization and fluctuations in the unconfined films, and Olympus ACT240TS silicon cantilevers ($k \sim 2$ N m^{-1}) for imaging defect annealing in the diblock films confined in channels. All imaging was performed using

AC or tapping mode in order to minimize the physical damage from the cantilever during imaging. The polymer heater mount situates the sample in direct contact with the heating element (300 to 700 K) while maintaining atmospheric control with a purging flow of room temperature argon. Drift correction allowed for imaging a single region of the film over long time periods.

The unconfined PS-*b*-PMMA films were prepared by spin coating a solution PS-*b*-PMMA (M_w = 77 kg mol^{-1}, Polymer Source) in toluene onto silicon nitride substrates, resulting in a 30 nm thick film. The scanning frame rate was between 30 to 180 s and the scan sizes ranged from 500 nm to 2 μm. For the films confined to channels, nanopatterns were introduced onto silicon nitride substrates using photoresist e-beam lithography then transferring the pattern to the substrate with a 95% CF_4, 5% O_2 plasma etch. The resulting etched channels are about 500 nm wide, 20 μm long, and 50 nm deep. After the substrates were cleaned, we spin coated a solution of PS-*b*-PMMA (M_w = 77 kg mol^{-1}, Polymer Source) in toluene at 4000–5500 rpm for 60 s. The films were then annealed at 523 K for 150 min under an inert argon atmosphere so that the PS-*b*-PMMA films formed well ordered aligned cylindrical domains with low defect density.

3. Results and discussion

3.1 Helium atom scattering as a probe of thin film polymer dynamics

The extension of HAS to the study of disordered films is complemented by improvements in the theoretical treatment of atom scattering from disordered surfaces.[13,14] In the case of a structurally disordered film, the nature of the scattering is quite different than from ordered surfaces. For structurally disordered surfaces there are no coherent diffraction channels available for scattering and thus the helium scatters diffusely. While there is no coherent scattering due to the absence of long-range order, there is still a rich palette of information available regarding the dynamical properties of such surfaces. Attenuation measurements of the elastically scattered fraction as well as analysis of the line shape of the inelastic features give insight into energy accommodation and momentum exchange in these gas-surface collisions. Furthermore, the nature of the gas-surface potential can be determined through careful analysis of the diffuse elastic and inelastically scattered components.

Time-of-flight spectroscopy was employed to observe the energy exchange characteristics of the PMMA surface, and a pseudorandom cross-correlation chopping technique was used to maximize signal-to-noise. Beam energies employed in this experiment range from 9.7 to 54 meV, with the sample temperatures ranging from 60 to 490 K, and scattering at the specular condition was performed for angles of 37.42°, 32.42°, and 24.42° from the surface normal. Fig. 1 shows an overlay of representative spectra at the specular condition as the surface temperature is varied. These spectra are comprised of a relatively sharp diffuse elastic peak (at cryogenic beam energies and sample temperatures from 60 to 120 K), and a broad inelastic, or multi-phonon, feature.

The attenuation of the elastic scattering component can be described theoretically using the Debye–Waller model.[9] The model relates the degree of the attenuation of the elastic component to the magnitude of the mean-square displacement (MSD) of the surface atoms or molecules from their equilibrium position. This analysis has been applied to the cases of metals,[15] self-assembled monolayers,[7] and organic crystals,[16] and in the case of PMMA we successfully demonstrate its application to a disordered polymer surface. In case of HAS, the elastically scattered component can be described by eqn (1) below, where the term $2W(T)$ is the Debye–Waller factor, I is the observed elastic intensity, and I_0 is the theoretical elastic intensity at $T_S = 0$ K. Eqn (2) defines the perpendicular and parallel momentum exchanges for the elastically scattered helium atoms, with the Beeby correction[17] accounting for the well depth, D, of the helium-polymer interaction potential, E_i the incident

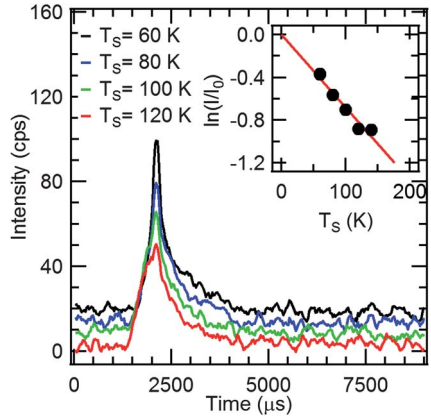

Fig. 1 Time-of-flight spectra at the specular condition from a 10 nm thick PMMA film with $E_B = 11$ meV and $\theta_i = 37.42°$ for sample temperatures ranging from 60 to 120 K. The elastic peak clearly decreases with sample temperature, and the inset shows a linear plot of the Debye–Waller factor *vs.* T_S.

helium atom kinetic energy, k_i the magnitude of the incident helium wave vector, and θ representing the angle from the surface normal for the incident (i) and scattered (f) helium atom wave vectors. The Debye–Waller factor itself can be separated into the contribution from perpendicular (z) and in plane ($\|$) displacements, and thus at specular scattering conditions the ΔK^2 term disappears and the attenuation is dependent only on displacements normal to the surface.

$$I = I_0 e^{-2W(T)}, 2W = \Delta k_z^2 \langle u_z^2 \rangle + \Delta K \langle u_\parallel^2 \rangle \quad (1)$$

$$\Delta k_z = k_i \left\{ \left[\cos^2(\theta_f) + \frac{D}{E_i} \right]^{\frac{1}{2}} + \left[\cos^2(\theta_i) + \frac{D}{E_i} \right]^{\frac{1}{2}} \right\}, \Delta K = k_i \left[\sin(\theta_f) - \sin(\theta_i) \right] \quad (2)$$

As is apparent from eqn (1), the temperature dependent thermal attenuation of the elastic feature can be used to characterize the MSDs arising from the surface vibrational modes. A plot of the natural log of the elastic intensity *versus* surface temperature is linear when the surface oscillators exhibit harmonic behavior and attenuation is due to the coarsening of the surface from thermal motion. Traditionally, this analysis is applied to the introduction of dynamic disorder in an ordered system, where a coherent elastic peak attenuates due to the coarsening of the ordered lattice. In the case of disordered polymer interfaces there is no ordered lattice and no coherent scattering is observed. Instead, the dynamic disorder at the surface attenuates diffuse elastic scattering intensity at a given solid angle by opening further diffuse scattering channels. We find that the Debye–Waller model fits the observed attenuation of our diffuse elastic peak intensity quite well, as seen in Fig. 1.

The inset of Fig. 1 shows the Debye–Waller plot of the spectra shown, and the linearity indicates that the harmonic approximation holds in the temperature regime studied. The fact that we are able to perform this analysis on a structurally disordered organic surface is impressive, but more remarkable is that this technique is sensitive to subtle changes in surface vibrations due to thin-film confinement. The peak intensity was taken as the height of the diffuse elastic peak, and the helium-polymer potential well depth was assumed to be 7 meV for this system since this value was experimentally obtained for high density alkanethiol self-assembled

monolayers.[7] The 10 nm PMMA samples had smaller MSDs ($6.0 \pm 0.5 \times 10^{-5}$ Å^{2}K^{-1}) than those of the thicker 50 nm films ($6.9 \pm 0.5 \times 10^{-5}$ Å^{2}K^{-1}). This reduced thermal motion due to thin film confinement has also been observed for bulk film MSDs by neutron scattering,[18] and possibly arises from strong substrate polymer interactions which can propagate to the interface in ultrathin films.

The multiphonon envelope line shape of the scattered helium also supports the Debye–Waller attenuation measurements in showing intrinsic differences in inelastic scattering profiles due to film thickness confinement effects. Since the 10 nm film is "stiffer" than the 50 nm film, it should show differences in its energy transfer profile. Fig. 2 overlays energy transfer profiles for both the 10 and 50 nm films at four different sample temperatures. It is interesting to note that the thicker film has more intensity attributed to annihilation events (the energy transfer scale is for the helium atom, thus a positive energy transfer is the atom gaining energy by annihilating surface vibrational modes) than the thinner film for all four sample temperatures. The suppression of thermal motion due to substrate interactions could account for the systematic differences observed in these energy transfer profiles.

The line shape of the multiphonon envelope was fit to the semi-classical theory developed by Manson, Celli, and Himes[13,14] to determine the nature of the gas-polymer potential. This model contains two situations for the nature of the potential, a continuum condition and a discrete scattering center condition. The continuum of atomic centers model has been applied to metal surfaces while the discrete model has been applied to an organic molecule monolayer. The differential reflection coefficient is shown in eqn (3), and the key component in our studies is the surface temperature dependent form factor prior to the exponential.

$$\frac{dR}{d\Omega_f dE_f} \propto |k_f||\tau_{fi}|^2 \left(\frac{\hbar\pi}{\omega_0 k_B T_S}\right)^n \exp\left[-\frac{(\Delta E + \hbar\omega_0)^2}{4k_B T_S \hbar\omega_0}\right] \quad (3)$$

The term τ_{fi} is the scattering transition matrix, which is the product of the Jackson-Mott matrix element of the surface potential and a parallel momentum cutoff term.[19] The classical recoil energy, $\hbar\omega_0$, is approximated as $\hbar^2\boldsymbol{k}^2/2M_{\text{eff}}$, where $\boldsymbol{k}$ is the total momentum transfer, $\boldsymbol{k}_f - \boldsymbol{k}_i$, and M_{eff} is the effective surface mass. The

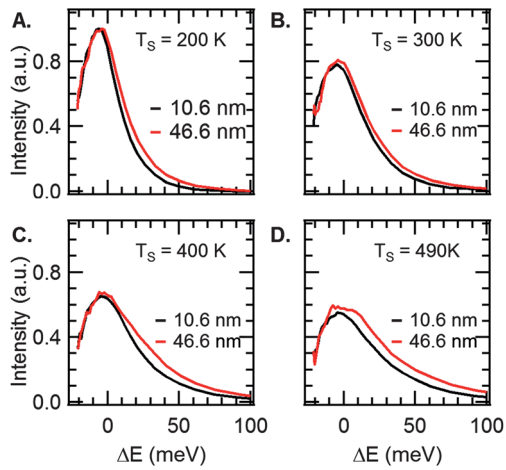

Fig. 2 Overlay of energy transfer spectra of a 31 meV beam comparing thin (black) and thick (red) PMMA films at four different sample temperatures at the specular condition $\theta_i = \theta_f = 24.42°$. As the sample temperature increases, the divergence in intensity of the annihilation (positive ΔE) side of the spectra increases.

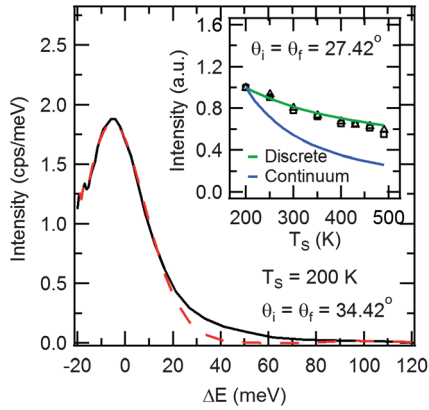

Fig. 3 An overlay of the experimental energy transfer spectrum of a 31 meV beam from the 47 nm PMMA film (black solid line) with the semiclassical discrete center model fit (red dashed line). The inset is the experimental intensity of the multiphonon feature at this beam energy for the thin (square) and thick (triangle) PMMA films compared to the semiclassical model predictions for the discrete (green) and continuum (blue) scattering potentials.

difference between the two models is in the power of the surface temperature dependence of the surface form factor, which is $n = 3/2$ for the continuum case and $n = 1/2$ for the discrete center case.

The PMMA multiphonon line shape is fit well by using the discrete model, and very poorly by the continuum model, as shown in Fig. 3. The only significant deviation from the model occurs in the high energy tail on the annihilation side of the spectra, which most likely arises from multiple scattering events not accounted for in this model. When the inelastic scattering profiles of polystyrene (PS) and polybutadiene (PB) were compared to PMMA, little difference was observed.[20] However, inherent differences in the multiphonon lineshape appear when scattering from polymer films of different molecular weight.[21]

3.2 Helium atom scattering as a probe of changes in dynamics due to phase transitions

The successful application of HAS for characterizing thin polymer film dynamics can be extended to more complex disordered systems, specifically those which undergo transitions between glassy and crystalline phases. The particular phase change polymer studied was poly(ethylene terephthalate), or PET, which undergoes a transition from a homogenous amorphous glass to a heterogeneous semi-crystalline film above its glass transition temperature (T_g), 348 K, and below its melt temperature of 523 K. The semi-crystalline film consists of crystalline lamellae comprised of stacked planes of *trans*-oriented polymer chains with amorphous domains between these lamellae. As in the case of thin polymer films, the sensitivity of helium atom scattering to surface thermal motion was employed to observe changes in surface vibrational dynamics due to a phase transition from an amorphous to a semi-crystalline PET film. The resulting Debye–Waller analysis truly demonstrates the power of helium atom scattering to detect subtle changes in interfacial dynamics.

Elastic scattering was observable at low beam energies (7.1 meV) and surface temperatures (40–120 K). The scattering profile from PET is similar to that of PMMA in that there is a sharp diffuse elastic feature and broader inelastic multiphonon component in the time-of-flight spectra. The Debye–Waller analysis was performed by fitting the elastic peak using a Gaussian function (FWHM ~1 meV) and the peak intensity was taken as the height of the elastic component fit. As in

the case with PMMA, the Beeby correction was assumed to have a well depth of 7 meV due to its use in similar systems.[7,16] Four independent measurements were made at each of five specular conditions ($\theta_i = \theta_f = 37.7°$, 33.7°, 29.7°, 25.7°, and 21.7°), and the normalized natural log of the peak intensities were averaged for each sample temperature at each kinematic condition. Using eqn (1) and (2), the perpendicular MSD was found to be $2.7 \pm 0.2 \times 10^{-4}$ Å^{2}K^{-1} for the amorphous surface and $3.1 \pm 0.1 \times 10^{-4}$ Å^{2}K^{-1} for the semi-crystalline interface (Fig. 4).

In-plane MSDs were characterized by measuring the thermal attenuation of the diffuse elastic peak at non-specular scattering conditions. Using the same beam energy, and the most glancing scattering condition ($\theta_i = 37.7°$), thermal attenuation measurements were performed at $\theta_f = 29.7°$ and 13.7°, which correspond to in-plane momentum exchanges of -0.43 Å^{-1} and -1.38 Å^{-1}, respectively. The perpendicular contributions to the Debye–Waller factor, as determined from the specular decay rate, are subtracted from the off-specular decay rate, leaving the Debye–Waller factor as a function of ΔK^2. An overlay of these decay rates at different non-specular conditions is presented in Fig. 5. The linear relationship between the decay rate and ΔK^2 confirms the efficacy of this analysis, and was used to extract the values for the in-plane MSD. The parallel MSD was $2.2 \pm 0.1 \times 10^{-3}$ Å^{2}K^{-1} for amorphous PET and $1.6 \pm 0.1 \times 10^{-3}$ Å^{2}K^{-1} for the semi-crystalline film.

Helium atom scattering is able to resolve a relatively small (~15%) but significant softening of the surface for the vibrations polarized perpendicular to the surface while detecting a 25% stiffening for the vibrations polarized in the surface plane due to a transition from a homogeneous amorphous film to a composite semi-crystalline film. This surprising and seemingly contradictory result can be explained by invoking the heterogeneous nature of the semi-crystalline film.[22,23] A polymer system which fully crystallizes, polyethylene (PE), was studied using neutron scattering and the crystalline film MSD was suppressed to 70% of the magnitude of those in the amorphous film.[24] Since fully crystalline polymers have reduced MSDs, the apparent softening of perpendicular MSDs in PET must arise from the remaining amorphous regions. Neutron scattering studies of fullerenes embedded in amorphous PS films have observed an enhancement of bulk MSDs despite the strong attractive potential of the fullerene, and this effect is attributed to frustrated packing of polymer chains away from the C_{60} molecules.[25] In PET, the tight polymer chain packing in the crystalline lamellae should prevent efficient chain packing in the remaining amorphous domains, much like C_{60} in PS. This frustrated polymer chain packing results in

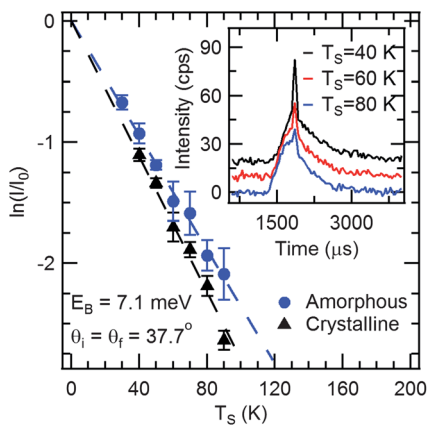

Fig. 4 Comparison of the Debye–Waller factor at the specular condition for amorphous and semicrystalline PET. The inset is an overlay of typical time-of-flight spectra at the three sample temperatures employed in this investigation.

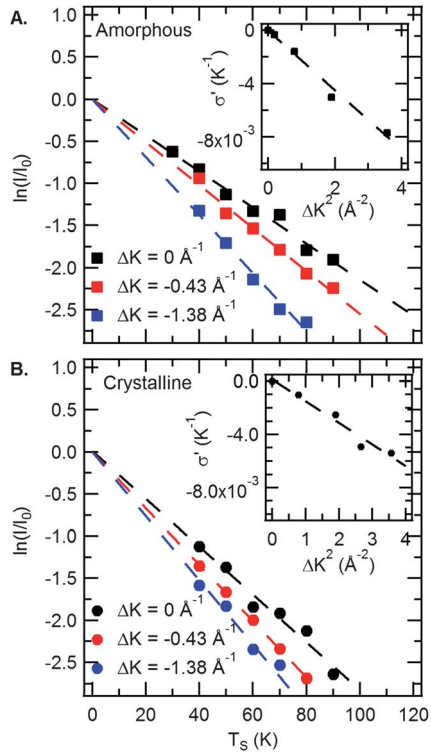

Fig. 5 Overlays of the Debye–Waller factor at specular and two non-specular conditions for amorphous (A) and semicrystalline (B) PET. The slope of the inset plots gives the in-plane mean-square displacements for the two surfaces.

a greater free volume and thus larger MSD in the interstitial amorphous regions, which explains the apparent softening of the PET interface upon crystallization.

As in the case of SAMs,[7] the parallel MSDs are an order of magnitude greater than those of the perpendicular polarization for both surfaces. The decrease of the in-plane MSD for the semi-crystalline film relative to the amorphous film originates from the crystalline lamellae. Since crystalline lamellae are more dense than the amorphous regions of the film, reduced free volume from the crystalline regions of the interface can explain this suppression of in-plane MSDs. These measurements support the presence of both crystalline lamellae and amorphous regions, distinct from those of the non-crystalline film, at the interface of this composite film.

3.3 Helium atom scattering as a probe of interfacial dynamics in a complex ordered film

The evolution of helium atom scattering as a probe of clean and adsorbate decorated surfaces continues as recently this technique has been used to study the structure, thermal motion, and specific librations of chemisorbed organic films.[7,8] We demonstrate the extension of this technique to a class of complex interfaces, best described as hybrid interfaces, in our studies of methyl-terminated silicon(111). Analysis of helium atom diffraction allows us to characterize the gas-surface potential, surface MSDs, and energy accommodation in gas-surface collisions. We also present the first observation of single phonon spectroscopy in methyl-terminated silicon, as well as the first observation of the lattice's vibrational band structure, through our inelastic HAS studies.

Methyl-terminated silicon is of great interest as it represents the next generation of passivated silicon interfaces. Since the early strategy of covalent termination by hydrogen lacked suitable resistance to oxidation, Lewis *et al.* developed a two step technique for covalently terminating the Si(111) interface with methyl units which results in high surface coverages.[12] Structural studies using low energy electron diffraction (LEED) and SPM techniques have confirmed the presence of large, pristine, highly ordered domains at this interface while transmission IR (TIR) and high resolution electron energy loss spectroscopy (HREELS) techniques were employed to characterize the molecular vibrations of the methyl terminated interface.[26–29] We present the use of Debye–Waller analysis and inelastic helium atom scattering to investigate the atomic scale librations, gas-surface collisional energy accommodation, and the vibrational dynamics of this hybrid interface.

Unlike the case for the disordered polymer films, CH_3–Si(111) gives intense, sharp diffraction peaks with minimal diffuse background. In this case, Debye–Waller formalism can be applied as a measurement of the dynamic disordering of an ordered lattice, which should arise due to the vibrations of both the methyl groups and the underlying silicon lattice. Rather than using time-of-flight spectroscopy to monitor the thermal attenuation of elastic scattering, we employed square wave chopping to make angularly resolved measurements yielding diffraction patterns at each given sample temperature. These scans show clearly resolved diffraction peaks which decay as the sample temperature increases, as seen in Fig. 6. This decay fits well with the Debye–Waller model of thermal attenuation not only in the linearity of the inset plot, but in that the diffraction peak decays at a much faster rate than the specular peak due to contributions from in-plane thermal motion. The parallel momentum exchange is defined by the elastic diffraction condition below, where h and k are integer indices for the reciprocal lattice unit vectors.

$$\Delta K = G = h\vec{b_1} + k\vec{b_2} \tag{4}$$

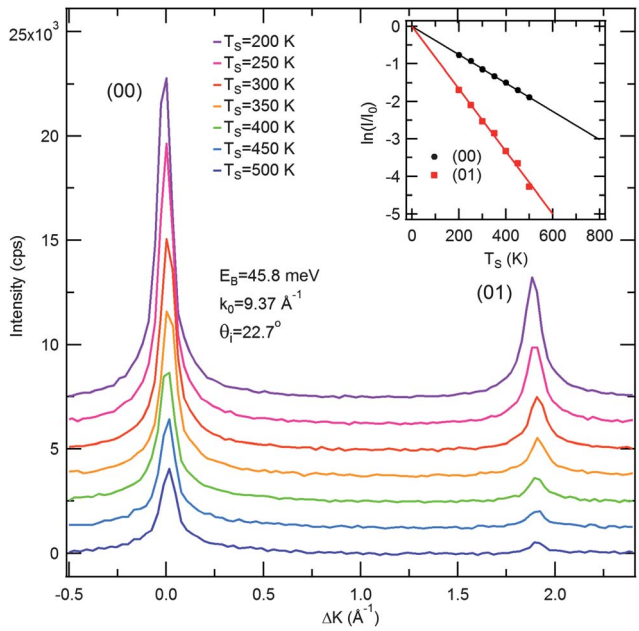

Fig. 6 Representative helium atom diffraction scans for a typical Debye–Waller attenuation experiment for CH_3–Si(111). The inset is the Debye–Waller factor *vs.* T_S for the zeroth and first order diffraction peaks.

For the CH_3–Si(111) surface the reciprocal lattice vector for the (01) diffraction peak was observed to be 1.90 $\AA^{-1}$, which corresponds to the 3.82 $\AA$ spacing of the underlying silicon lattice.

These diffraction peaks were fitted using two Gaussian functions to account for the narrow coherent elastic component as well as the broad multiphonon and diffuse scattering contributions, and the elastic intensity was extracted as the numerical integral of the elastic component of the two Gaussians. Repeat measurements of these thermal attenuation measurements were performed at five different specular conditions in order to elucidate the value for the He–CH_3–Si(111) well depth.

$$\sigma_{hk} \equiv -\frac{d(2W(T_S))}{dT_S} = -\Delta k_z^2 \frac{d\langle u_z^2\rangle}{dT_S} - \Delta K^2 \frac{d\langle u_\parallel^2\rangle}{dT_S} \tag{5}$$

In the case of the specular, or zeroth order, diffraction peak, the ΔK^2 term vanishes and the perpendicular component can be simplified to the form in eqn (6).

$$\Delta k_z^2 = 4k_i^2\left[\cos^2(\theta_i) + \frac{D}{E_i}\right] \tag{6}$$

As seen in Fig. 7D, a plot of σ_{00} *versus* $\cos^2(\theta_i)$ should be linear with an intercept that, when divided by the slope, gives the ratio of the Beeby well depth D to the incident beam energy. This method gave He-surface interaction potential well depths of 7.5 ± 2.6 meV and 6.0 ± 3.9 meV for the CH_3 and CD_3 terminated surfaces, respectively. It is worth noting that these values are in agreement with potentials applied to SAMs and methyl-terminated organic crystals,[7,16] and that although these values differ, they fall well within the precision of the method. We used the experimentally determined values for the well depths of each surface, but note that using the average of the two values changes our calculated MSD by less than 5% due to the large beam energy used relative to D.

Analysis of these rates of thermal attenuation of the elastic diffraction peaks allowed the quantification of the perpendicular and parallel MSDs for both surfaces. The perpendicular MSD was $1.0 \pm 0.1 \times 10^{-5}$ $\AA^2K^{-1}$ and $1.2 \pm 0.2 \times 10^{-5}$ $\AA^2K^{-1}$ for the respective CH_3 and CD_3 surfaces. The enhancement of the mean-square displacement in the CD_3 surface is in accordance with the expected impact of isotopic substitution. Eqn (7) details how the surface Debye temperature (θ_D) can be extracted from σ_{00}, given that the surface temperature is within the order of θ_D.

$$\sigma_{00} = \frac{24m_{He}[E\cos^2(\theta_i) + D]}{M_{eff}k_B\theta_D^2} \tag{7}$$

There are two unknown parameters in this equation, M_{eff} and θ_D, so the appropriate treatment of mass is necessary in order to quantify the surface Debye temperature. Scattering studies from silica glass[30] found the effective surface mass to be

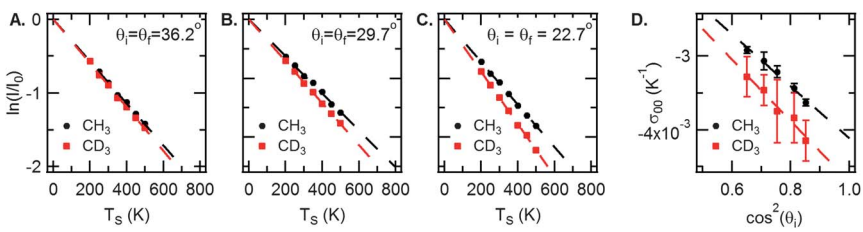

Fig. 7 Comparison of representative specular decays at three different incident angles (A–C) with fits (dashed lines) for the CH_3 and CD_3 terminated surfaces. Fig. 7D is the plot of the specular decay rate, with fits, as a function of $\cos^2(\theta_i)$ for CH_3–Si(111) and CD_3–Si(111). The intercept is used to extract the He-surface potential well depth.

18 amu, or roughly the mass of a hydroxyl unit terminating the surface, so we employed the mass of the terminal methyl group for our analysis. This assumption combined with the experimentally observed well depths resulted in a surface Debye temperature of 983 ± 31 K, or 683 cm^{-1}, for the CH_3 surface ($M_{eff} = 15$ amu) and 824 ± 40 K, or 573 cm^{-1}, for the CD_3 surface ($M_{eff} = 18$ amu). These values are both higher than the Debye temperature of bulk silicon (645 K) and that of the estimate for the Si(111) surface (476 K),[31] and much higher than those observed for organic thin films.[32,33] The HREELS measurements of the molecular vibrational modes of the CH_3–Si(111) surface[27,28] indicate that the Si–C stretching mode is 680 cm^{-1}, which corresponds to 980 K. While no spectroscopic data are available on the vibrational modes of the CD_3–Si(111) surface, comparison to spectroscopic studies of gas phase CD_3SiH_3 and CD_3SiD_3 can be helpful. The gas phase Si–C stretch is 700 cm^{-1} for CH_3SiH_3, 645 cm^{-1} for CD_3SiH_3 and 619cm^{-1} for CD_3SiD_3, so further suppression of the mode's energy due to the mass of the second layer of silicon could easily depress this value into the range of 570 cm^{-1}.[34]

Covalent methyl termination appears to have stiffened the surface in the normal polarization, and the surface Debye temperatures indicate that the Si–C stretching mode dominates the thermal motion and energy accommodation at this interface. The relatively low perpendicular MSD also implies a stiffer surface, since its magnitude is closer to that of a rigid semiconductor or metal than that of a thin organic film. Enhancement of the surface Debye temperature by the addition of an organic adlayer has been observed.[35] These results demonstrate the sensitivity of helium atom scattering to changes in the local chemical environment.

The parallel MSDs were obtained from the σ_{hk} for the first and second order diffraction peaks. These attenuation rates were averaged to obtain a parallel MSD of 7.1 ± 5.1 × 10^{-4} $Å^2K^{-1}$ for CH_3–Si(111) and 7.2 ± 5.3 × 10^{-4} $Å^2K^{-1}$ for CD_3–Si(111). While the perpendicular MSDs resembled those of a rigid semiconductor, these values are consistent with those observed in other thin organic films.[7,36] The addition of a single methyl functional group was sufficient to transition the interfacial dynamics from a regime mediated by substrate lattice vibrations to one in which the thermal motion and energy accommodation is dominated by local molecular modes.

The thermal motion is dominated by local molecular modes for the methyl-terminated silicon interface, but the lattice dynamics are still accessible through inelastic helium atom scattering. Since the first observation of the surface waves of an alkali halide using helium atom scattering,[3] the use of helium atom scattering to investigate the surface vibrational structure has been extended to increasingly complex interfaces.[37,38] Knowledge of the surface phonon band structure allows for the characterization of the local bonding character of the interface, so inelastic helium atom scattering enables us to investigate how the local silicon bonding is affected by the covalent attachment of a methyl terminal group. We report the first helium atom scattering measurements of lattice vibrational modes of not only CH_3–Si(111), but any semiconductor system with covalent termination by an organic functional group.

For this set of experiments a single shot chopping method was employed, with a duty cycle of 1% and beam energies ranging from 35 to 64 meV. Typical sample temperatures ranged from 140 K to 200 K to reduce the attenuation from diffuse scattering. A representative time-of-flight spectrum is shown in Fig. 8 with an inset of the Rayleigh wave dispersion curve along the $\bar{\Gamma} - \bar{M}$, or nearest neighbor, azimuth for the CD_3–Si(111) surface. This spectrum consists of a weak diffuse elastic peak (relative to the coherent diffraction peaks) and a clear inelastic peak with a longer flight time than the elastic peak, corresponding to the creation of a surface vibration during collision. Changing the kinematic conditions at a given beam energy allows us to map out the dispersion of these interfacial vibrational modes across the surface Brillouin zone. The vibrational structure resembles that observed for the H–Si(111) surface,[37] so methyl termination not only preserves the underlying

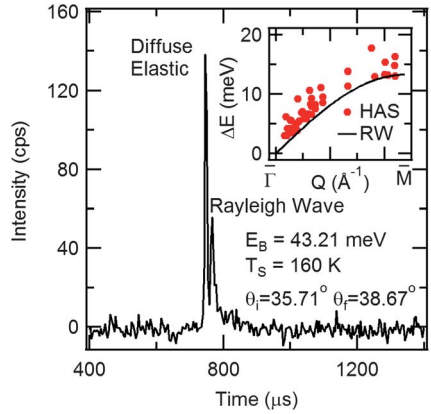

Fig. 8 A time-of-flight spectrum demonstrating single phonon inelastic helium scattering from CD_3–Si(111). The inelastic peak arises from a creation event with the surface Rayleigh wave. The inset is the Rayleigh wave dispersion along the $\bar{\Gamma} - \bar{M}$ azimuth (nearest neighbor) for the CD_3–Si(111) surface.

lattice structure but also its low energy vibrational band structure. The low frequency of the surface modes accessible by helium atom scattering means that these modes are unlikely to mix significantly with the molecular modes of the methyl groups. This does not exclude the possibility of an altered band structure for the higher frequency lattice modes, but in the case of the Rayleigh wave it is relatively unperturbed. An important clarification is that while we are probing lattice vibrational modes using helium atom scattering, we are not in fact scattering from the silicon lattice itself. The helium atom scattering is non-penetrative, so this motion is projected from the underlying lattice onto the surface methyl groups.

In summary, helium atom scattering experiments discussed herein demonstrate the power of this technique in characterizing and quantifying surface vibrations in disordered and complex systems. We have demonstrated its sensitivity to subtle changes in surface librations due to local environmental effects arising from confinement (*i.e.* thickness) and substrate interactions, phase change, and chemical functionalization. Furthermore, we have demonstrated the utility of using the temperature and angle dependent attenuation of elastically scattered atoms to gain fundamental insights on energy accommodation in gas-solid collisions for hybrid interfaces.

3.4 Mechanisms of defect migration and annihilation in aligned diblock copolymers

As a complement to our atomic scattering data, we now discuss our use of high temperature time-lapse atomic force microscopy to obtain real-space images of mesoscopic phase separation, chain diffusion, and structural reorganization in diblock copolymer films. Diblock copolymer systems are of great technological interest due to their self-organizing behavior, which has been used for a variety of applications,[39,40] and earlier atomic force microscopy investigations of the structural evolution in diblock copolymers involved *ex situ* heating and static imaging below T_g.[41–43] While these studies gave useful insight into the structural organization and defect migration of these films, they did not yet allow direct imaging of the domain fluctuations or reorganization in real time. Time-lapse AFM imaging above T_g gives *in situ* real-space observations of such behavior in diblock copolymer films, which allows a more complete characterization of the mechanisms directing structural evolution and fluctuations. Previously we used this method to demonstrate that direct visualization of PS-*b*-PMMA domain fluctuation and growth, Fig. 9, allows

us to determine that domain boundaries fluctuate through polymer chain tube-like reptation and are most likely restored by a curvature minimization force.[44]

Previous studies have used time-lapse atomic force microscopy measurements to study coarsening processes in polymer films, but they were limited by complicated structure of phase-separated diblock copolymer films.[45,46] Our innovation is to use lithographically modified substrates to enforce a highly ordered cylindrical domain alignment and lower defect densities.[39] The low defect densities afford us the luxury of studying *isolated defect interactions* while the alignment enables us to study the migration of these defects both along and across domain boundaries. Our high temperature imaging studies offer insight into the energy barriers and mechanism for defect migration and annihilation in these complex polymer films.

In this paper, we focus on the interactions of isolated dislocations and disclinations, Fig. 10. These defects can migrate through a combination of climb (diffusion along a domain interface) and glide (diffusion across a domain interface) mechanisms, which have been predicted by theory but not directly observed due to the disordered nature of the previous films studied. Both mechanisms should be involved in the film reorganization, but the climb should have a much higher velocity than the glide mechanism due to the large energetic cost from repulsion of immiscible domains. The linear cylindrical alignment in this study allows for the direct observation of both the climb and glide mechanism velocities through our time-lapse AFM images.

Dislocations of opposite orientation will attract and annihilate leaving a defect-free region of the film. This annihilation proceeds with a combination of glide and climb mechanisms as seen in Fig. 11. Note that the velocity along the domain interface is much higher than across, as predicted for climb and glide mechanisms. Detailed observation of the glide and climb mechanism velocities allows for the characterization of their respective diffusion constants as well as quantification of the activation barrier to defect diffusion. Disclinations do not move with the same mechanisms as the dislocations due to the topological constraints, so they must

Fig. 9 Sequential AFM phase images at 448 K showing PMMA domain (dark) fluctuations within the PS matrix (light).

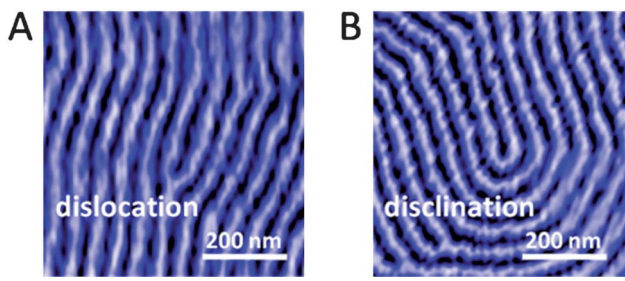

Fig. 10 Examples of topological defects which are observed in cylinder-forming PS-*b*-PMMA films. A shows a dislocation and B a disclination with a PMMA core structure. PMMA domains appear dark and PS domains appear bright in the AFM phase image.

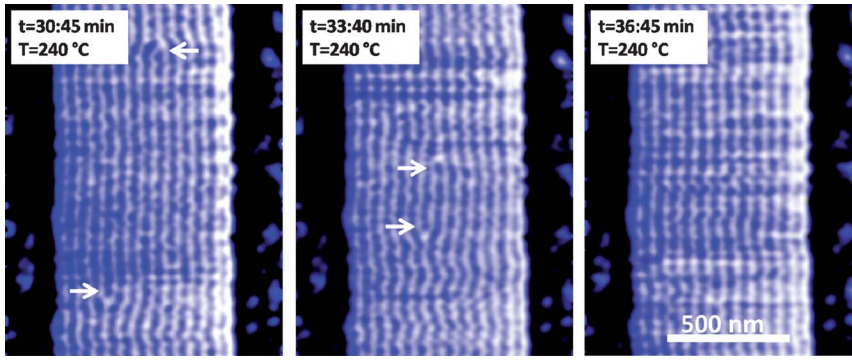

Fig. 11 Representative AFM phase images showing the annihilation of a dislocation pair. The dislocations are indicated with white arrows. The images were acquired at 513 K.

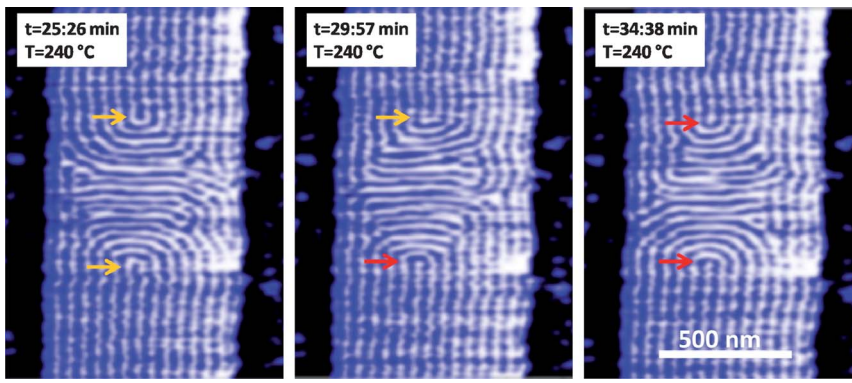

Fig. 12 AFM images showing the attraction of a disclination quadrupole. The yellow arrows correspond to the PMMA disclination cores, while the red arrows correspond to the PS disclination cores. These images were acquired at 513 K.

migrate *via* domain breaking and reorganization. Fig. 12 shows the approach of two oppositely oriented disclinations. The yellow arrows correspond to a PMMA disclination core while the red arrows correspond to a PS disclination core. The disclinations migrate by breaking the disclination lines into dislocations, which then are free to interact with the surrounding domains and annihilate, and then switching the disclination core structure between PS and PMMA. While we were not able to observe dislocation emission, which should quench rapidly, we are able to visualize the core-switching component of this mechanism quite clearly. This mechanism was predicted theoretically[47] but has not been previously observed. Our ability to make direct observations of film reorganization and defect migration has led to greater insights into the precise energetics and kinetics involved in diblock copolymer film annealing.

4. Conclusions

In this paper we have shown that helium atom scattering can be applied as a precision probe of surface vibrational dynamics and gas-surface interaction potentials to disordered and complex macromolecular films as well as to a hybrid interface. We demonstrated the ability of helium atom scattering to detect subtle changes in surface vibrational dynamics due to thin film confinement, polymer chain molecular weight, and phase through our studies of PMMA and PET films. Helium atom

scattering also allowed us to characterize the surface thermal motion, gas-surface energy accommodation, and the interfacial lattice dynamics of a hybrid interface, methyl-terminated silicon. Time-lapse atomic force microscopy complemented our atom scattering studies by allowing *in situ* real space imaging of mesoscopic structural evolution in PS-*b*-PMMA, a diblock copolymer film. By employing a lithographically modified substrate, we were able to use cylindrical alignment of polymer domains to directly observe isolated defect pair migration both along and across domain boundaries, as well as the mechanism of annihilation. Helium atom scattering and time-lapse atomic force microscopy are powerful complementary tools, which together give profound insight into interfacial dynamics at atomic, nanoscopic, and microscopic length scales for complex condensed matter interfaces.

Acknowledgements

We would like to thank Nathan S. Lewis, Erik Johansson, and Leslie E. O'Leary at the California Institute of Technology for providing us with high quality methyl-terminated silicon samples. This work was supported at the University of Chicago by the Air Force Office of Scientific Research, DTRA (Grant No. HDTRA1-11-1-0001), and the NSF Materials Research Science and Engineering Center at the University of Chicago.

References

1 I. Estermann and O. Stern, *Z. Phys.*, 1930, **61**, 95.
2 M. J. Cardillo, G. E. Becker, S. J. Sibener and D. R. Miller, *Surf. Sci.*, 1981, **107**, 469.
3 G. Brusdeylins, R. B. Doak and J. P. Toennies, *Phys. Rev. Lett.*, 1980, **44**, 1417.
4 B. Poelsema and G. Comsa, *Faraday Discuss. Chem. Soc.*, 1985, **80**, 247.
5 K. D. Gibson and S. J. Sibener, *Phys. Rev. Lett.*, 1985, **55**, 1514.
6 F. Hofmann and J. P. Toennies, *Chem. Rev.*, 1996, **96**, 1307.
7 N. Camillone, C. E. D. Chidsey, G. Y. Liu, T. M. Putvinski and G. Scoles, *J. Chem. Phys.*, 1991, **94**, 8493.
8 S. B. Darling, A. M. Rosenbaum and S. J. Sibener, *Surf. Sci.*, 2001, **478**, L313.
9 D. Farias and K. H. Rieder, *Rep. Prog. Phys.*, 1998, **61**, 1575.
10 B. Gans, P. A. Knipp, D. D. Koleske and S. J. Sibener, *Surf. Sci.*, 1992, **264**, 81.
11 Y. Zhang, Y. L. Lu, Y. X. Duan, J. M. Zhang, S. K. Yan and D. Y. Shen, *J. Polym. Sci., Part B: Polym. Phys.*, 2004, **42**, 4440.
12 A. Bansal, X. L. Li, I. Lauermann, N. S. Lewis, S. I. Yi and W. H. Weinberg, *J. Am. Chem. Soc.*, 1996, **118**, 7225.
13 J. R. Manson, V. Celli and D. Himes, *Phys. Rev. B: Condens. Matter*, 1994, **49**, 2782.
14 J. R. Manson and J. G. Skofronick, *Phys. Rev. B: Condens. Matter*, 1993, **47**, 12890.
15 V. Bortolani, V. Celli, A. Franchini, J. Idiodi, G. Santoro, K. Kern, B. Poelsema and G. Comsa, *Surf. Sci.*, 1989, **208**, 1.
16 G. Bracco, J. Acker, M. D. Ward and G. Scoles, *Langmuir*, 2002, **18**, 5551.
17 J. L. Beeby, *J. Phys. C: Solid State Phys.*, 1971, **4**, L359.
18 C. L. Soles, J. F. Douglas, W. L. Wu and R. M. Dimeo, *Macromolecules*, 2003, **36**, 373.
19 M. B. Li, J. R. Manson and A. P. Graham, *Phys. Rev. B: Condens. Matter*, 2002, **65**, 195404.
20 M. A. Freedman, J. S. Becker, A. W. Rosenbaum and S. J. Sibener, *J. Chem. Phys.*, 2008, **129**, 044906.
21 M. A. Freedman, J. S. Becker and S. J. Sibener, *J. Phys. Chem. B*, 2008, **112**, 16090.
22 T. Kanaya, M. Imai and K. Kaji, *Phys. B*, 1996, **226**, 82.
23 D. A. Ivanov, T. Pop, D. Y. Yoon and A. M. Jonas, *Macromolecules*, 2002, **35**, 9813.
24 T. Kanaya, U. Buchenau, S. Koizumi, I. Tsukushi and K. Kaji, *Phys. Rev. B: Condens. Matter*, 2000, **61**, R6451.
25 A. Sanz, M. Ruppel, J. F. Douglas and J. T. Cabral, *J. Phys.: Condens. Matter*, 2008, **20**, 104209.
26 L. J. Webb, S. Rivillon, D. J. Michalak, Y. J. Chabal and N. S. Lewis, *J. Phys. Chem. B*, 2006, **110**, 7349.
27 T. Yamada, T. Inoue, K. Yamada, N. Takano, T. Osaka, H. Harada, K. Nishiyama and I. Taniguchi, *J. Am. Chem. Soc.*, 2003, **125**, 8039.

28 T. Yamada, M. Kawai, A. Wawro, S. Suto and A. Kasuya, *J. Chem. Phys.*, 2004, **121**, 10660.
29 H. B. Yu, L. J. Webb, R. S. Ries, S. D. Solares, W. A. Goddard, J. R. Heath and N. S. Lewis, *J. Phys. Chem. B*, 2005, **109**, 671.
30 W. Steurer, A. Apfolter, M. Koch, W. E. Ernst, E. Sondergard, J. R. Manson and B. Holst, *Phys. Rev. B: Condens. Matter Mater. Phys.*, 2008, **78**, 045427.
31 J. S. Ha and E. F. Greene, *J. Chem. Phys.*, 1989, **91**, 571.
32 J. J. Hernandez, J. A. Li, J. Baker, S. A. Safron and J. G. Skofronick, *J. Vac. Sci. Technol., A*, 1996, **14**, 1788.
33 C. N. Borca, S. Adenwalla, J. W. Choi, P. T. Sprunger, S. Ducharme, L. Robertson, S. P. Palto, J. L. Liu, M. Poulsen, V. M. Fridkin, H. You and P. A. Dowben, *Phys. Rev. Lett.*, 1999, **83**, 4562.
34 A. J. F. Clark and J. E. Drake, *Can. J. Spectrosc.*, 1977, **22**, 79.
35 D. Q. Feng, P. A. Dowben, R. Rajesh and J. Redepenning, *Appl. Phys. Lett.*, 2005, **87**, 181918.
36 T. Y. B. Leung, P. Schwartz, G. Scoles, F. Schreiber and A. Ulman, *Surf. Sci.*, 2000, **458**, 34.
37 R. B. Doak, Y. J. Chabal, G. S. Higashi and P. Dumas, *J. Electron Spectrosc. Relat. Phenom.*, 1990, **54**, 291.
38 P. Santini, P. Ruggerone, L. Miglio and R. B. Doak, *Phys. Rev. B: Condens. Matter*, 1992, **46**, 9865.
39 D. Sundrani, S. B. Darling and S. J. Sibener, *Nano Lett.*, 2004, **4**, 273.
40 R. A. Segalman, *Mater. Sci. Eng., R*, 2005, **48**, 191.
41 T. L. Morkved, W. A. Lopes, J. Hahm, S. J. Sibener and H. M. Jaeger, *Polymer*, 1998, **39**, 3871.
42 J. Hahm, W. A. Lopes, H. M. Jaeger and S. J. Sibener, *J. Chem. Phys.*, 1998, **109**, 10111.
43 J. Hahm and S. J. Sibener, *J. Chem. Phys.*, 2001, **114**, 4730.
44 N. A. Yufa, J. Li and S. J. Sibener, *Macromolecules*, 2009, **42**, 2667.
45 C. Harrison, D. H. Adamson, Z. D. Cheng, J. M. Sebastian, S. Sethuraman, D. A. Huse, R. A. Register and P. M. Chaikin, *Science*, 2000, **290**, 1558.
46 C. Harrison, Z. D. Cheng, S. Sethuraman, D. A. Huse, P. M. Chaikin, D. A. Vega, J. M. Sebastian, R. A. Register and D. H. Adamson, *Phys. Rev. E: Stat. Phys., Plasmas, Fluids, Relat. Interdiscip. Top.*, 2002, **66**, 011706.
47 N. M. Abukhdeir and A. D. Rey, *New J. Phys.*, 2008, **10**, 063025.